(Received 24 June 2025, Accepted 8 August 2025, Scheduled 22 August 2025)

Compact MSL-Fed CWG Polarizer Using Corner-Truncated Patch

Ir-Ving Tseng and Chun-Long Wang*

National Taiwan University of Science and Technology, Taipei 106335, Taiwan

ABSTRACT: In this paper, a compact microstrip line (MSL)-to-circular waveguide (CWG) transition using a rectangular patch is introduced. As the rectangular patch is placed 2.68 mm ($0.043\lambda_g$) away from the short-circuited plane of the CWG, the transition is very compact. By truncating the rectangular patch of the compact MSL-to-CWG transition, a compact MSL-fed CWG polarizer using the corner-truncated patch is proposed. The proposed polarizer has a compact size and a phase difference of -90.97° at 9.65 GHz. The axial ratio is within ± 1 dB from 8.5 GHz to 10 GHz. The reflection coefficient is smaller than -10 dB from 9.03 GHz to 10.5 GHz. In addition, as the corner-truncated patch is adopted, the proposed polarizer does not require a complex manufacturing process on the waveguide. Moreover, as the microstrip line feeds the polarizer, it can be easily integrated with other planar circuits. To verify the simulation results, the MSL-fed CWG polarizer using the corner-truncated patch is fabricated and measured. The simulation and measurement results are in good agreement.

1. INTRODUCTION

Microstrip line (MSL)-to-circular waveguide (CWG) transitions are commonly used in the feeding of circular waveguides. As circular waveguides and rectangular waveguides have similar electromagnetic field distributions, techniques used in the design of microstrip line (MSL)-to-rectangular waveguide (RWG) transitions can be straightforwardly applied to the design of MSL-to-CWG transitions. At the beginning, MSL-to-RWG transitions can be formed by using multi-section ridged waveguides [1], tapered ridged waveguides [2], or multi-section rectangular waveguides [3, 4]. However, these structures are bulky, heavy, and expensive. To reduce the cost, some scholars use an antisymmetric gradient fin line to complete the MSL-to-RWG transition [5]. This transition uses a planar circuit to complete the transition, which can greatly reduce the production cost, but the area occupied by the gradient fin line is quite large. To reduce the area of the transition, some scholars use quarter-wavelength probes combined with relay transitions [6–9] to complete the MSL-to-RWG transition. Although the area occupied by the quarter-wavelength probe is quite small, various relay transitions are added which increase the area of the transition. In addition, other scholars use quarter-wavelength probes combined with quarter-wavelength short-circuit rectangular waveguides [10–14] to complete the MSL-to-RWG transition. Although the area occupied by the quarter-wavelength probe is quite small, an additional quarter-wavelength short-circuit rectangular waveguide is added which increases the area of the transition. In addition, some scholars use a quarter-wavelength probe combined with a rectangular waveguide resonant cavity [15] or a rectangular waveguide wedge [16] to complete an MSL-to-RWG transition. Although the area occupied by the quarter-wavelength probe is quite small, adding a rectangular waveguide resonant cavity or rectangular waveguide wedge will increase the area of the transition and increase the cost of rectangular waveguide production. To achieve miniaturized transitions, some scholars use a quarter-wavelength bow-tie antenna [17] or an antisymmetric tapered probe [18] to complete a miniaturized MSL-to-RWG transition. The size of these transitions is quite small, only a quarter of a wavelength in length. Though the techniques mentioned above have also been applied to high-frequency MSL-to-RWG transitions [19–21], the size of the transition is still of a quarter wavelength. To further reduce the size of the transition, a compact MSL-to-CWG transition using a rectangular patch is introduced. As the rectangular patch is placed 2.68 mm ($0.043\lambda_g$) away from the short-circuited plane of the CWG, the transition is very compact.

Circular waveguide (CWG) polarizers have been widely discussed over the past few centuries. First, some scholars used multiple grooves to achieve CWG polarizers [22]. In addition, some scholars used metal irises to achieve CWG polarizers [23, 24]. Although these types of CWG polarizers have a very wideband response, they require complex machining to complete the metal grooves or irises, which raises the production cost. To reduce the production cost, some scholars used metal partitions to achieve CWG polarizers [25–27]. However, because the largest electric field of the CWG TE_{11} mode is at the center of the CWG polarizer, placing the metal partition at the center of the CWG polarizer will cause greater reflection. To reduce reflection, some scholars used a dielectric septum to replace metal partitions so that a CWG polarizer using the dielectric septum is formed [28]. Although the use of a dielectric septum can achieve lower reflection, it requires a very long dielectric septum, thus increasing the size of the CWG polarizer.

In the above designs, there is a need for the energy to be fed into the CWG so that the CWG polarizer may work properly. Therefore, some scholars proposed a metal column CWG

* Corresponding author: Chun-Long Wang (clw@mail.ntust.edu.tw).

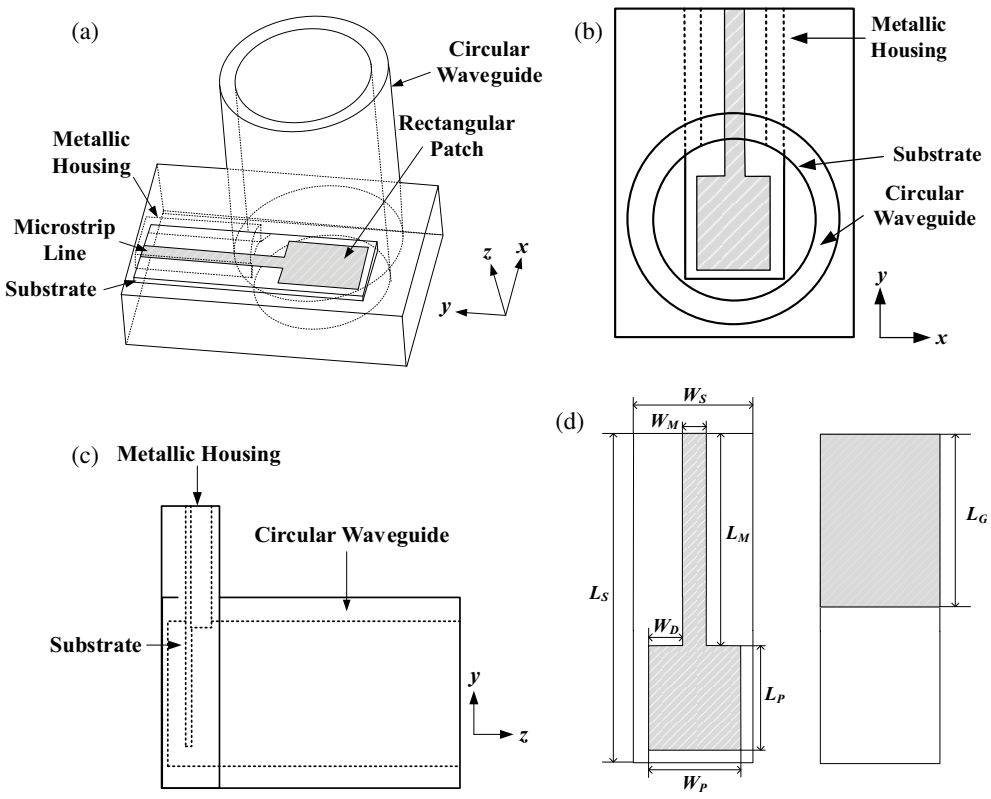

FIGURE 1. The MSL-to-CWG transition using the rectangular patch. (a) The schematic view. (b) The xy-cross-sectional view. (c) The yz-cross-sectional view. (d) Top and bottom views of the planar circuit.

polarizer fed by a coaxial cable [29]. This design combines coaxial cable-to-CWG transition and CWG polarizer using a metal column. As a result, the overall volume of the coaxial cable-fed CWG polarizer is quite large. To reduce the volume, some scholars proposed a mesh metal CWG polarizer fed by a coaxial cable [30]. This design combines coaxial cable-to-CWG transition and CWG polarizer using a mesh metal. As a result, the overall volume is reduced. Even so, as this design directly connects two microwave components in series, one is the transition and the other the CWG polarizer, the volume required by two separate microwave components is substantially larger. To reduce the volume of this integrated system, a miniaturized MSL-to-CWG transition is designed and then transformed into an MSL-fed CWG polarizer. As a result, the feeding system to the CWG and CWG polarizer can be integrated as a compact component, leading to a volume reduction of the overall system. To achieve the above objective, an MSL-to-CWG transition using a metal patch is proposed in Section 2. The volume occupied by this transition is very small as the metal patch is directly attached to the end of the CWG. To transform the transition into a CWG polarizer, the metal patch is cut at the corners to achieve an MSL-fed CWG polarizer using a truncated metal patch in Section 3. So far, the MSL-to-CWG transition and CWG polarizer have been integrated into a compact single component. Compared with the designs in [29, 30], it is discovered that this integrated MSL-fed CWG polarizer has a very small volume because the truncated metal patch can be directly attached to the end of the CWG.

2. COMPACT MSL-TO-CWG TRANSITION USING RECTANGULAR PATCH

2.1. Transition Topology

A compact MSL-to-CWG transition using a rectangular patch is proposed as shown in Fig. 1, where Fig. 1(a) shows the schematic view; Fig. 1(b) shows the *xy*-cross-sectional view; Fig. 1(c) shows the *yz*-cross-sectional view; and Fig. 1(d) shows the top and bottom views of the planar circuit. As shown in Fig. 1, the microstrip line port and circular waveguide port are matched. The proposed transition consists of a circular waveguide, a metallic housing, and a planar circuit. The radius of the circular waveguide is selected as 10.5 mm so that the cutoff frequency of the dominant TE_{11} mode is 8.53 GHz and the cutoff frequency of the first higher-order TM_{01} mode is 10.77 GHz. To ensure that only the TE_{11} dominant mode propagates in the circular waveguide while the other higher-order modes of the CWG are still below cutoff, the operation bandwidth of the CWG is chosen between 8.53 GHz and 10.77 GHz. In accordance, the cross-sectional dimensions of the metallic housing for the microstrip line are chosen as $3.2 \times 8.4\,\text{mm}^2$ so that there would be only microstrip line mode propagation in the frequency range from 8.53 GHz to 10.77 GHz, while all the waveguide modes of the metallic housing are below cutoff. The planar circuit intrudes the CWG by the side so that the electric field of the rectangular patch will be matched to that of the electric field of the CWG, which will be described later. Besides, since the planar circuit is placed at only 2.68 mm $(0.043\lambda_g)$

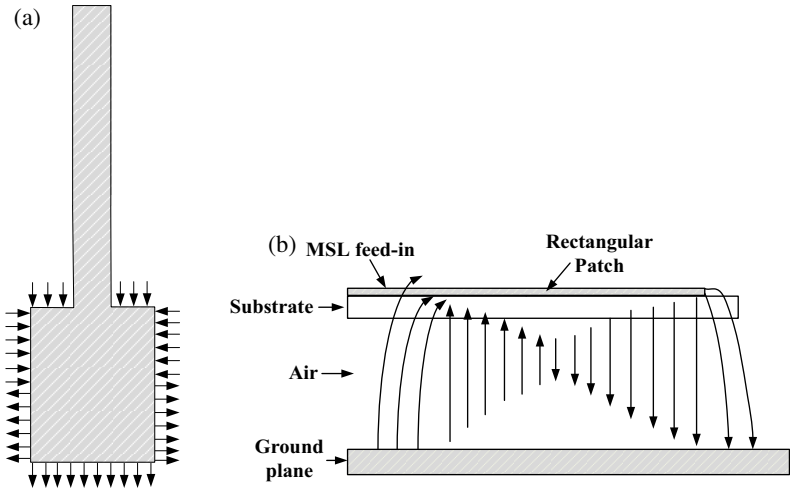

FIGURE 2. The electric field distribution of the rectangular patch. (a) The electric field distribution around the peripheral of the rectangular patch. (b) The yz-cross-sectional view of the electric field distribution of the rectangular patch.

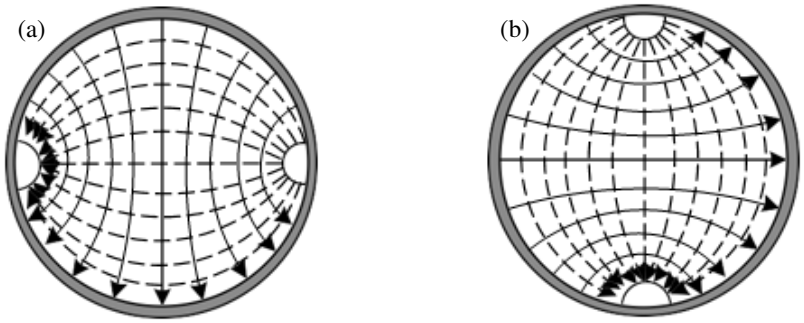

FIGURE 3. E-field (solid line) and H-field (dashed line) distributions of the TE_{11} mode of the circular waveguide. (a) Vertically-polarized CWG. (b) Horizontally-polarized CWG.

away from the short-circuited end of the circular waveguide, which serves as the ground plane of the rectangular patch, the proposed transition is compact.

Fig. 1(d) shows the top and bottom views of the planar circuit, which consists of the microstrip feed-in and rectangular patch. The planar circuit is fabricated on an RT/Duroid 5880 substrate with a relative dielectric constant of 2.2 and a thickness of 0.8 mm. The microstrip feed-in has a characteristic impedance of 50 Ω, which conforms to the commonly used standard impedance. By simply controlling the length of the patch, the operating frequency of the transition can be determined.

The electric field distribution of the rectangular patch is shown in Fig. 2, where the electric field distribution around the peripheral of the rectangular patch is shown in Fig. 2(a), and the yz-cross-sectional view of the electric field distribution of the rectangular patch is shown in Fig. 2(b). Fig. 3 shows the E-field and H-field distributions of the TE_{11} mode for the vertically-polarized CWG and horizontally-polarized CWG. As can be observed from Fig. 1(b), since the rectangular patch is aligned with the cross-section of the CWG, the electric field distribution in Fig. 2(a) would only excite the vertically-polarized CWG shown in Fig. 3(a). The horizontally-polarized CWG shown in Fig. 3(b) would not be excited as the electric field distributions on the right and left sides of the rectangular patch are in opposite polarities in Fig. 2(a).

2.2. Design and Analysis of the Transition

Reconsidering Fig. 1, since the characteristic impedance of the microstrip line is chosen to be 50 Ω, the width of the microstrip line W_M can be calculated to be 2.48 mm, and the length of the microstrip line is arbitrarily given as 17.7 mm. Since the center frequency is 9.65 GHz, which is the average of 8.53 GHz and 10.77 GHz, the rectangular patch length L_P can be estimated to be half the wavelength of the frequency $f_c = 9.65$ GHz, which is 12.5 mm [32]. All the other parameters are given in Table 1. To determine the value of the patch width W_P, The MSL-to-CWG transition using the rectangular patch in Fig. 1, along with the dimensions listed in Table 1, is simulated with Ansoft High Frequency Structure Simulator (HFSS) by varying the patch width W_P. The frequency response of the reflection coefficient for the MSL-to-CWG transition using the rectangular patch with various patch widths W_P is shown in Fig. 4. As can be seen from Fig. 4, when the patch width W_P increases, the corresponding resonance frequency decreases slightly. The patch width W_P is chosen as 9.3 mm, resulting in a small re-

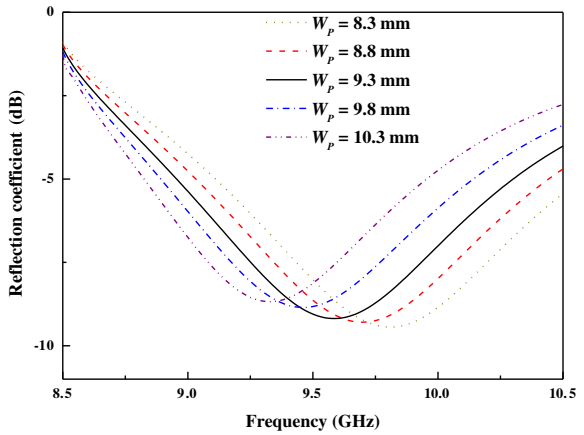

FIGURE 4. The frequency response of the reflection coefficient for the MSL-to-CWG transition using the rectangular patch with various patch widths W_P.

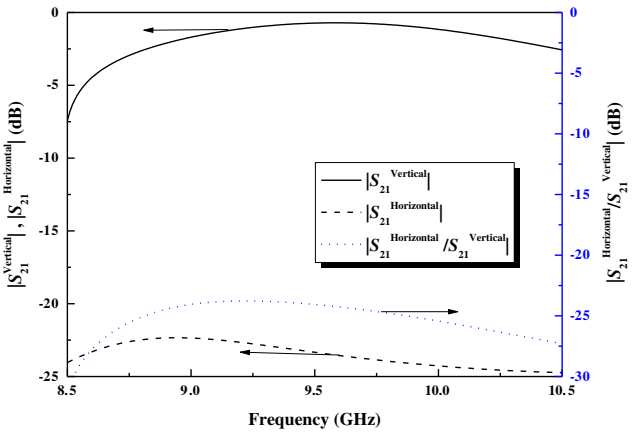

FIGURE 5. The frequency responses of the vertically-polarized and horizontally-polarized transmission coefficients for the MSL-to-CWG transition using the rectangular patch.

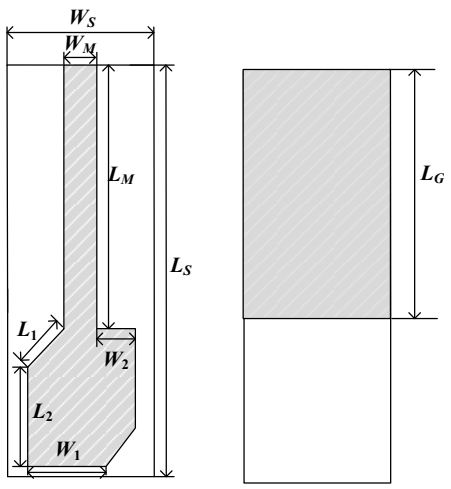

FIGURE 6. Top and bottom views of the MSL-fed CWG polarizer using the corner-truncated patch.

TABLE 1. The dimensions of the MSL-to-CWG transition using the rectangular patch. Unit: mm.

L_S	L_M	L_P	L_G
34	20.37	12.5	17.7
W_S	W_M	W_P	W_D
12.5	2.48	9.3	3.51

flection coefficient at 9.65 GHz. To demonstrate that the rectangular patch will only excite the vertically-polarized TE_{11} mode, the frequency responses of the vertically-polarized and horizontally-polarized transmission coefficients for the MSL-to-CWG transition using the rectangular patch are shown in Fig. 5. As can be seen from Fig. 5, the horizontally-polarized transmission coefficient can be ignored as it is -25 dB smaller than that of the vertically-polarized transmission coefficient within the frequency range 8.5 to 10.5 GHz.

3. MSL-FED CWG POLARIZER USING CORNER-TRUNCATED PATCH

3.1. Polarizer with Matched CWG Port

The MSL-fed CWG polarizer using the corner-truncated patch has the same structure as the MSL-to-CWG transition using the rectangular patch shown in Fig. 1(a), except that the rectangular patch is now truncated. The microstrip line port and circular waveguide port are matched. The top and bottom views of the planar circuit for the MSL-fed CWG polarizer using the corner-truncated patch are depicted in Fig. 6. By comparing Fig. 6 with Fig. 1(d), the only difference between the MSL-fed CWG polarizer and MSL-to-CWG transition is that the corners of the rectangular patch are truncated. As a result, the descriptions of the polarizer shown in Fig. 6 are the same as those of the transition shown in Fig. 1, which have been addressed in Section 2.1.

As can be seen from the electric field distribution around the peripheral of the rectangular patch shown in Fig. 2(a), the electric field distributions of the up and low edges of the rectangular patch will excite the vertically-polarized CWG. In contrast, the electric field distributions of the right and left edges tend to cancel with each other, leading to diminished horizontally-polarized CWG. To alleviate the cancellation between the electric field distributions of the right and left edges, the rectangular patch is truncated diagonally, where L_{C1} represents the truncated length on the up and low edges and L_{C2} represents the truncated length on the right and left edges. The remaining electric field distributions are shown in Fig. 7. As can be seen from Fig. 7, part of the electric field on the peripheral of the patch is eliminated, making the electric field more balanced in the vertical and horizontal directions. As can be observed from Fig. 7, the leading phase of the electric field on the low edge (point R) should have a 90-degree phase advance over the leading phase of the electric field on the left edge (point S) to achieve a right-hand circularly-polarized (RHCP) wave. As a result, the following relationship should be satisfied.

$$\beta(W_P - L_{C1}) = 90^\circ \tag{1}$$

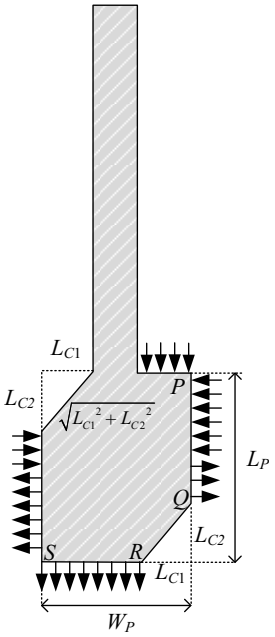

FIGURE 7. The electric field distribution around the peripheral of the corner-truncated patch.

Besides, since the total phase of the peripheral of the truncated patch should be 360 degrees, the following relationship should be satisfied.

$$\beta\left[(L_P - L_{C2}) + \sqrt{L_{C1}^2 + L_{C2}^2} + (W_P - L_{C1})\right] = 180^\circ \tag{2}$$

By dividing Equation (2) by Equation (1), the following equation is obtained.

$$\frac{(L_P - L_{C2}) + \sqrt{L_{C1}^2 + L_{C2}^2} + (W_P - L_{C1})}{2(W_P - L_{C1})} = 1 \tag{3}$$

Equation (3) can be manipulated to solve for the truncated length L_{C2} on the left edge of the patch shown below.

$$L_{C2} = \frac{(\Delta l)^2 + 2(\Delta l)L_{C1}}{2(\Delta l) + 2L_{C1}} \tag{4}$$

where $\Delta l = L_P - W_P$. By arbitrarily giving the truncated length L_{C1} on the up edge of the patch, the required truncated length L_{C2} on the left edge of the patch can be acquired.

Given the truncated length L_{C1} =3.5 mm and $\Delta l = L_P - W_P = 12.5 - 9.3 = 3.2$ mm, the required truncated length L_{C2} can be calculated to be 2.43 mm through using Equation (4). With the truncated lengths $L_{C1} = 3.5$ mm and $L_{C2} = 2.43$ mm, The MSL-fed CWG polarizer using the corner-truncated patch in Fig. 1(a) and Fig. 7, along with the other dimensions listed in Table 1, is simulated by using Ansoft HFSS, and the frequency response of the phase difference between the vertically-polarized and horizontally-polarized transmission coefficients for the MSL-fed CWG polarizer using the corner-truncated patch is shown in Fig. 8. As can be seen from Fig. 8, the phase difference is only -81.12°, which deviates

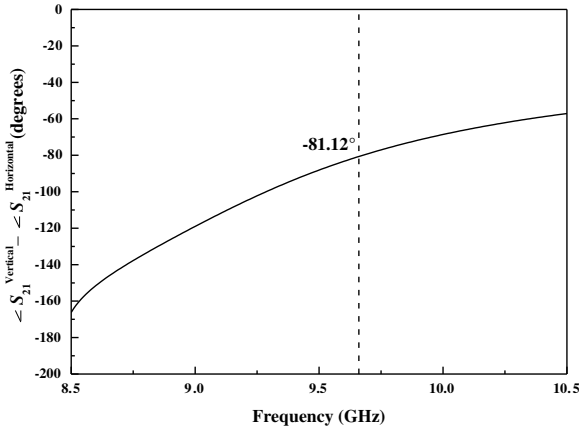

FIGURE 8. The frequency response of the phase difference between the vertically-polarized and horizontally-polarized transmission coefficients for the MSL-fed CWG polarizer using the corner-truncated patch. $L_P = 12.5$ mm, $L_{C1} = 3.5$ mm, and $L_{C2} = 2.43$ mm.

from the required value of -90° at the center frequency $f_0 = 9.65$ GHz. To compensate the deviation in the phase difference, the dimensions of the corner-truncated patch are optimized. The patch length L_P is changed from 12.5 mm to 13.1 mm; the truncated length L_{C1} on the up edge of the patch remains as $L_{C1} = 3.5$ mm; the truncated length L_{C2} on the left edge of the patch is changed from 2.43 mm to 3.7 mm. The MSL-fed CWG polarizer using the corner-truncated patch in Fig. 1(a) and Fig. 7, along with the optimized dimensions, is simulated by using the Ansoft HFSS, and the phase difference between the vertically-polarized and horizontally-polarized transmission coefficients for the MSL-fed CWG polarizer using the corner-truncated patch now becomes -90.97° at the center frequency $f_0 = 9.65$ GHz. The final dimensions of the MSL-fed CWG polarizer using the corner-truncated patch are summarized in Table 2.

Figure 9 shows the frequency response of the axial ratio for the MSL-fed CWG polarizer using the corner-truncated patch. As can be seen from Fig. 9, the axial ratio is within ± 1 dB from 8.5 GHz to 10 GHz. Besides, the axial ratio is 0.002 dB

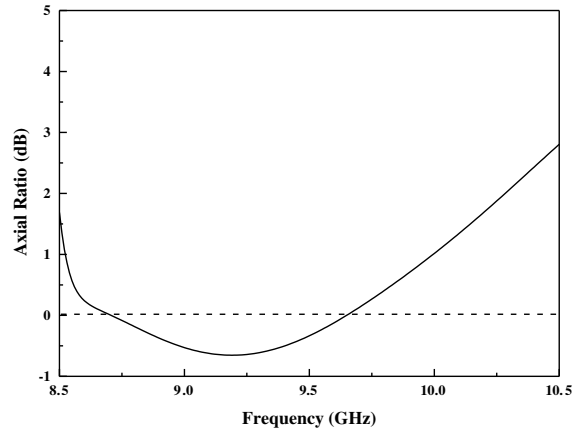

FIGURE 9. The frequency response of the axial ratio for the MSL-fed CWG polarizer using the corner-truncated patch. $L_P = 13.1$ mm, $L_{C1} = 3.5$ mm, and $L_{C2} = 3.7$ mm.

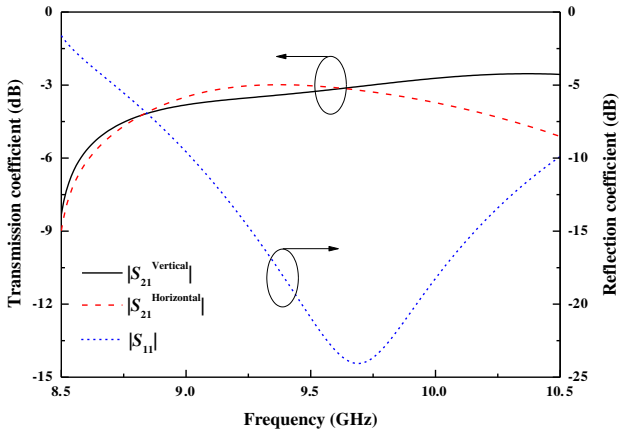

FIGURE 10. The frequency response of the vertically-polarized and horizontally-polarized transmission coefficients and the reflection coefficient for the MSL-fed CWG polarizer using the corner-truncated patch. $L_P = 13.1$ mm, $L_{C1} = 3.5$ mm, and $L_{C2} = 3.7$ mm.

TABLE 2. The final dimensions of the MSL-fed CWG polarizer using the corner-truncated patch. Unit: mm.

L_S	L_M	L_1	L_2	L_G
35	20.37	5.3	9.4	17.7
W_S	W_M	W_1	W_2	
12.5	2.48	5.79	3.31	

at the center frequency $f_0 = 9.65$ GHz. The frequency response of the vertically-polarized and horizontally-polarized transmission coefficients for the MSL-fed CWG polarizer using the corner-truncated patch is shown in Fig. 10. As can be seen from Fig. 10, the vertically-polarized and horizontally-polarized transmission coefficients take similar values below 10 GHz. At the center frequency $f_0 = 9.65$ GHz, each of them gets an equal -3-dB half-power, so the sum of them is equal to 0 dB. However, when the frequency is above 10 GHz, the vertically-polarized transmission coefficient tends to be much larger than the horizontally-polarized transmission coefficient, causing the axial ratio to deviate more from 0 dB as shown in Fig. 9. The frequency response of the reflection coefficient for the MSL-fed CWG polarizer using the corner-truncated patch is shown in Fig. 10. As can be seen from Fig. 10, the reflection coefficient is smaller than -10 dB from 9.03 GHz to 10.5 GHz.

3.2. Polarizer with Opened CWG Port

To gain the radiation patterns of the right-hand circularly-polarized (RHCP) and left-hand circularly-polarized (LHCP) waves, the CWG port of the MSL-fed CWG polarizer using the corner-truncated patch shown in Fig. 1(a) and Fig. 6 is now opened. The MSL-fed CWG polarizer using the corner-truncated patch in Fig. 1(a) and Fig. 6, along with the dimensions listed in Table 1, is simulated by using Ansoft HFSS with the CWG port opened. The simulated radiation patterns of the RHCP and LHCP waves at $f = 9.65$ GHz are shown in Fig. 11. As can be seen from Fig. 11, the magnitude of the electric field of the RHCP wave is 14.97 dB larger than the magnitude of

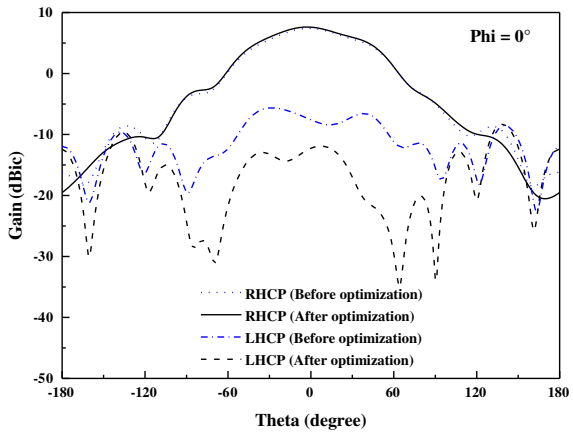

FIGURE 11. Comparison between the radiation patterns for the original and optimized polarizers at $f = 9.65$ GHz.

the electric field of the LHCP wave at $\theta = 0°$. Consequently, the radiation pattern is mainly RHCP. The radiation patterns of the RHCP and LHCP waves can be used to generate the phase difference between $\angle E_\varphi$ and $\angle E_\theta$, which could be obtained by [31]

$$\angle E_\phi - \angle E_\theta = \angle\left(j\frac{E_{RHCP} - E_{LHCP}}{E_{RHCP} + E_{LHCP}}\right) \tag{5}$$

The phase difference between $\angle E_\theta$ and $\angle E_\phi$ at 9.65 GHz is shown in Fig. 12, where the phase difference at $\theta = 0°$ shifts to $-69.34°$, which is far from $-90°$. Besides, the magnitudes of the electric fields of the RHCP and LHCP waves can then be used to calculate the value of the axial ratio, which is defined as the major axis to the minor axis of the polarization ellipse [31].

$$AR = \frac{|E_{RHCP} + E_{LHCP}|}{|E_{RHCP} - E_{LHCP}|} \tag{6}$$

The resulting axial ratio calculated from the RHCP and LHCP waves at $f = 9.65$ GHz is shown in Fig. 13. As can be seen from Fig. 13, the axial ratio is smaller than 7 dB when the value of θ is within $\pm 95°$. The corresponding 7-dB axial ratio beamwidth is 190°. Fig. 14 shows the frequency response of

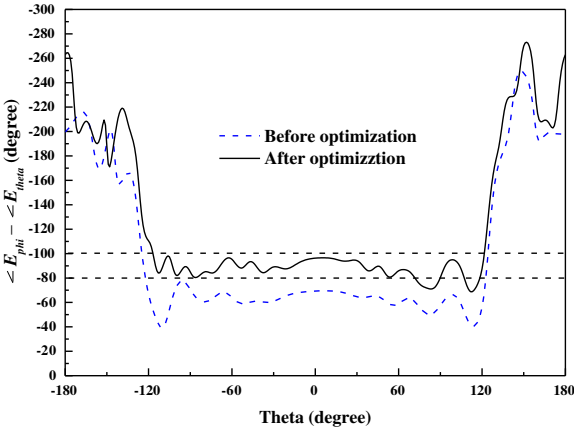

FIGURE 12. Comparison between the phase differences for the original and optimized polarizers at $f = 9.65$ GHz.

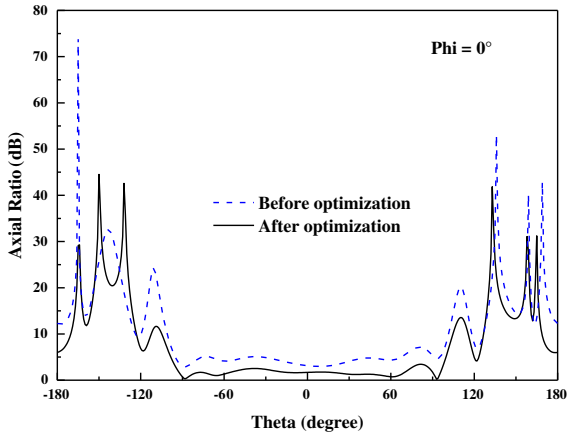

FIGURE 13. Comparison between the axial ratios for the original and optimized polarizers at $f = 9.65$ GHz.

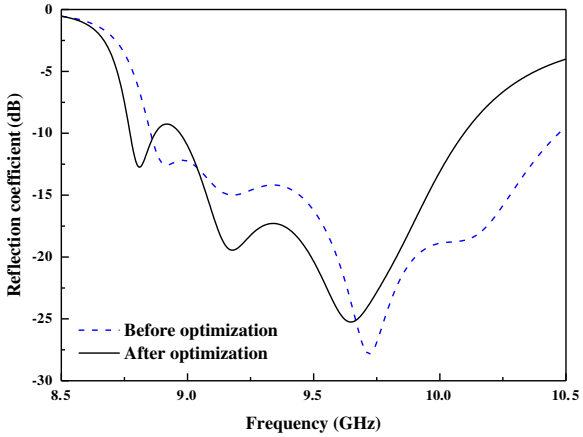

FIGURE 14. Comparison between the frequency responses of the reflection coefficients for the original and optimized polarizers.

the reflection coefficient for the MSL-fed CWG polarizer using the corner-truncated patch when the CWG port is opened. As can be seen from Fig. 14, the bandwidth, for which the reflection coefficient is smaller than -10 dB, covers from 8.86 GHz to 10.47 GHz.

As can be seen from Fig. 12 and Fig. 13, the axial ratio falls away from 0 dB, and the phase difference falls away from $-90°$ when the CWG port is opened. These deviations can be reduced by improving the radiation patterns of RHCP over LHCP waves shown in Fig. 11. To improve the radiation patterns of RHCP over LHCP waves, the truncated lengths L_{C1} and L_{C2} shown in Fig. 7 are optimized. Fig. 15 shows the top and bottom views of the optimized MSL-fed CWG polarizer using the corner-truncated patch when the CWG port is opened. The optimized dimensions are listed in Table 3. Fig. 15, along with the dimensions listed in Table 3, is simulated by using the Ansoft HFSS, and the radiation patterns of the RHCP and LHCP waves for the optimized polarizer at $f = 9.65$ GHz are shown in Fig. 11. As can be seen from Fig. 11, the magnitude of the electric field of the RHCP wave is now 19.85 dB larger than the magnitude of the electric field of the LHCP wave at $\theta = 0°$. The phase difference for the optimized polarizer at 9.65 GHz is shown in Fig. 12. As can be seen from Fig. 12, the phase difference at $\theta = 0°$ improves from -69.34 degrees to -96 degrees, and the phase difference within $90° \pm 10°$ corresponds to $\theta = -117°$ to $71°$. The axial ratio for the optimized polarizer at $f = 9.65$ GHz is shown in Fig. 13. As can be seen from Fig. 13, when the value of θ is within $\pm 95°$, the axial ratio is now reduced from 7 dB to 3.5 dB. The frequency response of the reflection coefficient for the optimized polarizer is shown in Fig. 14. As can be seen from Fig. 14, the reflection coefficient is smaller than -10 dB from 8.97 GHz to 10.1 GHz.

TABLE 3. The dimensions of the optimized MSL-fed CWG polarizer using the corner-truncated patch. Unit: mm.

L_S	L_M	L_1	L_2	L_G
35	21.77	3.53	9.95	17.53
W_S	W_M	W_1	W_2	W_3
12.5	2.48	7.1	3.56	1.06

4. VERIFICATIONS

To verify the simulation results, the optimized MSL-fed CWG polarizer using the corner-truncated patch in Fig. 1(a) and Fig. 15 is fabricated as shown in Fig. 16. To gain the radiation patterns, the fabricated polarizer in Fig. 16 is measured by using the Wavepro NSI2000 near-field system in Fig. 17. The comparison between the simulated and measured radiation patterns for the optimized polarizer at $f = 9.65$ GHz is displayed in Fig. 18. The simulated and measured radiation patterns in Fig. 18 can be used to generate the simulated and measured phase differences for the optimized polarizer at $f = 9.65$ GHz in Fig. 19 through (5). The simulated and measured phase differences are in good agreement except for θ beyond $\pm 120°$, which may be caused by the misalignment while setting up the measurement instrument. Furthermore, the simulated and measured radiation patterns in Fig. 18 can also be used to generate

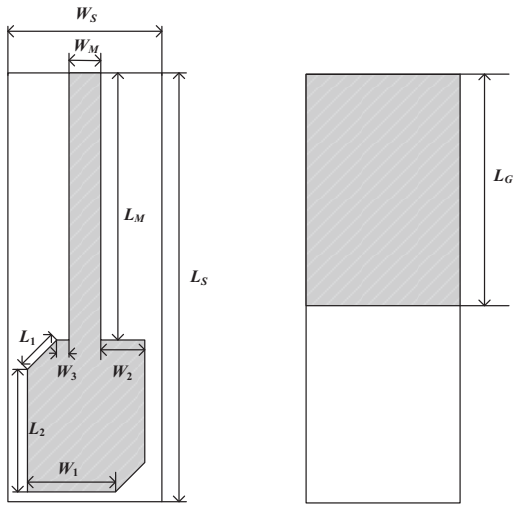

FIGURE 15. Top and bottom views of the optimized MSL-fed CWG polarizer using the corner-truncated patch when the CWG port is opened.

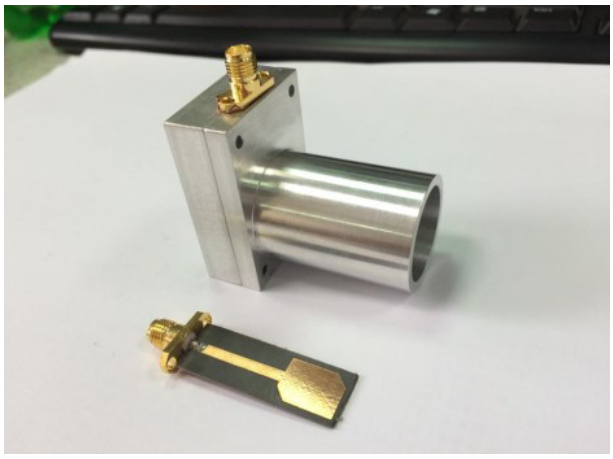

FIGURE 16. Photograph of the assembled polarizer.

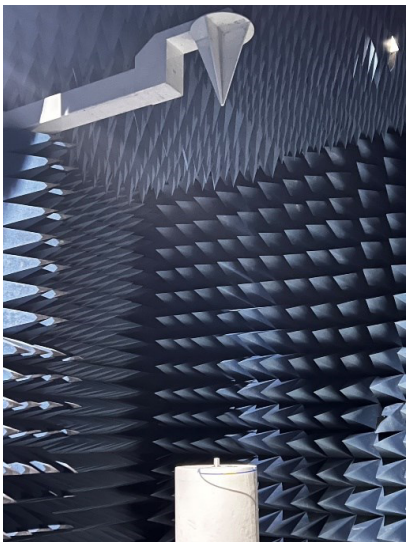

FIGURE 17. Photograph of radiation pattern measurement setup.

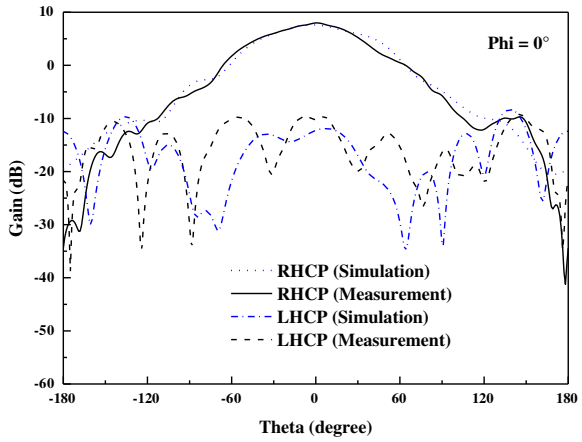

FIGURE 18. Comparison between the simulated and measured radiation patterns for the optimized polarizer at $f = 9.65$ GHz.

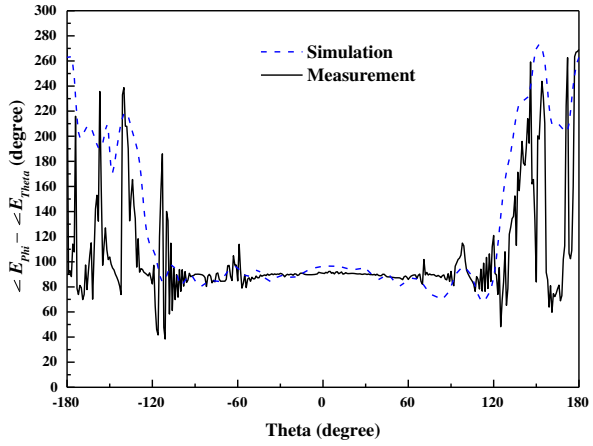

FIGURE 19. Comparison between the simulated and measured phase differences for the optimized polarizer at $f = 9.65$ GHz.

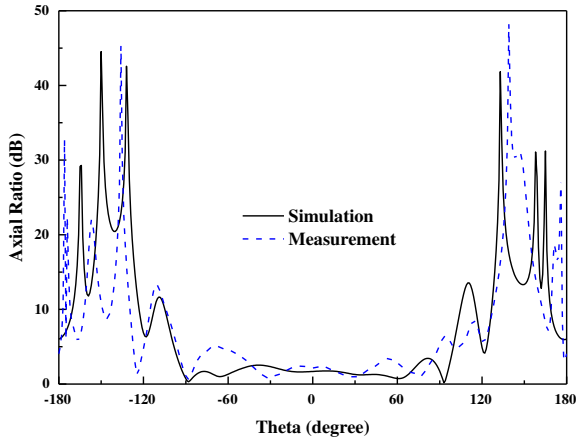

FIGURE 20. Comparison between the simulated and measured axial ratios for the optimized polarizer at $f = 9.65$ GHz.

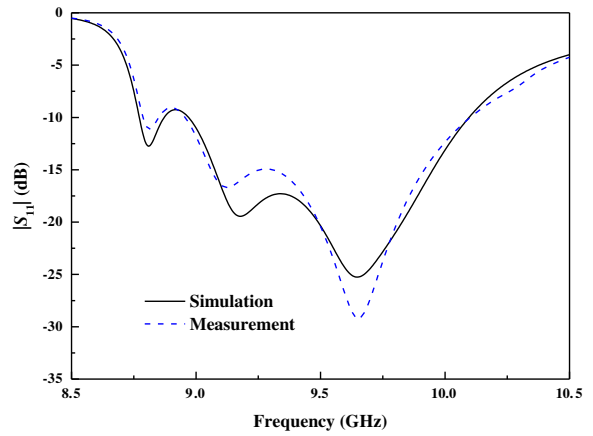

FIGURE 21. Comparison between the simulated and measured frequency responses of the reflection coefficients for the optimized polarizer.

TABLE 4. Comparison of the polarizers with feeding.

Type of Polarizer	*Operation Band (GHz)*	*Length of the Circuit (mm)*	*Return Loss (dB)*	*Axial Ratio (dB)*
Coaxial-fed polarizer using metal posts [29]	8.0–8.6	50	20	2.5
Coaxial-fed polarizer using wire reflector [30]	8.15–8.83	25.5	10	6
MSL-fed polarizer using truncated patch	9.03–10.5	3.48	10	3

the simulated and measured frequency responses of the axial ratios for the optimized polarizer in Fig. 20 through (6). The simulated and measured minimum axial ratios are in good agreement.

To gain the frequency response of the reflection coefficient, the fabricated polarizer in Fig. 16 is then measured by using Agilent E8362B PNA (10 MHz–20 GHz) after the short-open-load through (SOLT) calibration process is done. The comparison between the simulated and measured frequency responses of the reflection coefficients for the optimized polarizer is shown in Fig. 21. The simulated and measured reflection coefficients are in good agreement.

5. CONCLUSION

This paper proposes a compact MSL-to-CWG transition using a rectangular patch. Because the rectangular patch is located 2.68 mm $(0.043\lambda_g)$ from the CWG short-circuit plane, this transition is compact. Furthermore, by appropriately truncating the rectangular patch in this compact MSL-to-CWG transition, a compact MSL-fed CWG polarizer using the truncated patch can be realized. Because the transition and polarizer are integrated into a single component, no additional feeding structure for the polarizer is required. As a result, the MSL-fed CWG polarizer itself is extremely compact. The proposed polarizer exhibits a phase difference of $-90.97°$ at 9.65 GHz. The axial ratio is within ± 1 dB in the 8.5 GHz to 10 GHz range. The reflection coefficient is less than -10 dB in the 9.03 GHz to 10.5 GHz range. To validate the simulation results, an MSL-fed CWG polarizer using the truncated patch was fabricated and measured. The simulated results are highly consistent with the measured ones. Table 4 provides a comparison of the polarizers, and it can be seen that the polarizer proposed in this paper has the smallest circuit length.

ACKNOWLEDGEMENT

This work was supported in part by the National Science and Technology Council, Taiwan, under Grant NSTC 114-2221-E-011-075. The authors would like to thank Wireless Communications & Applied Electromagnetic LAB, National Taiwan University of Science and Technology, for providing the simulation environment of Ansoft® HFSS V.13 and the measurement instruments.

REFERENCES

[1] Yao, H.-W., A. Abdelmonem, J.-F. Liang, and K. A. Zaki, "Analysis and design of microstrip-to-waveguide transitions," *IEEE Transactions on Microwave Theory and Techniques*, Vol. 42, No. 12, 2371–2380, 1994.

[2] Hannachi, C., T. Djerafi, and S. O. Tatu, "Broadband E-band WR12 to microstrip line transition using a ridge structure on high-permittivity thin-film material," *IEEE Microwave and Wireless Components Letters*, Vol. 28, No. 7, 552–554, 2018.

[3] Pérez, J. M., A. Rebollo, R. Gonzalo, and I. Ederra, "An inline microstrip-to-waveguide transition operating in the full W-band based on a Chebyshev multisection transformer," *Journal of Infrared, Millimeter, and Terahertz Waves*, Vol. 36, No. 8, 734–744, 2015.

[4] Pérez Escudero, J. M., A. E. Torres-García, R. Gonzalo, and I. Ederra, "A simplified design inline microstrip-to-waveguide transition," *Electronics*, Vol. 7, No. 10, 215, 2018.

[5] Li, J., Y. Huang, Y. Li, G. Wen, and F. Xiao, "Wideband transition between rectangular waveguide and microstrip using asymmetric fin line probe," *Electronics Letters*, Vol. 53, No. 7, 490–492, 2017.

[6] Lin, T.-H. and R.-B. Wu, "A broadband microstrip-to-waveguide transition with tapered CPS probe," in *2002 32nd European Microwave Conference*, 1–4, Milan, Italy, 2002.

[7] Lou, Y., C. H. Chan, and Q. Xue, "An in-line waveguide-to-microstrip transition using radial-shaped probe," *IEEE Microwave and Wireless Components Letters*, Vol. 18, No. 5, 311–313, 2008.

[8] Kaneda, N., Y. Qian, and T. Itoh, "A broad-band microstrip-to-waveguide transition using quasi-Yagi antenna," *IEEE Transactions on Microwave Theory and Techniques*, Vol. 47, No. 12, 2562–2567, 2002.

[9] Kim, J., W. Choe, and J. Jeong, "Submillimeter-wave waveguide-to-microstrip transitions for wide circuits/wafers," *IEEE Transactions on Terahertz Science and Technology*, Vol. 7, No. 4, 440–445, 2017.

[10] Shih, Y.-C., T.-N. Ton, and L. Q. Bui, "Waveguide-to-microstrip transitions for millimeter-wave applications," in *1988 IEEE MTT-S International Microwave Symposium Digest*, 473–475, New York, NY, USA, 1988.

[11] Zaman, A. U., V. Vassilev, P.-S. Kildal, and H. Zirath, "Millimeter wave *E*-plane transition from waveguide to microstrip line with large substrate size related to mmic integration," *IEEE Microwave and Wireless Components Letters*, Vol. 26, No. 7, 481–483, 2016.

[12] Li, E. S., G.-X. Tong, and D. C. Niu, "Full W-band waveguide-to-microstrip transition with new *E*-plane probe," *IEEE Mi-*

crowave and Wireless Components Letters, Vol. 23, No. 1, 4–6, 2013.

[13] Lin, C.-C. and Y.-J. Hwang, "Single-sleeve waveguide-to-microstrip transition probe for full waveguide bandwidth," in *2012 42nd European Microwave Conference*, 766–769, Amsterdam, Netherlands, 2012.

[14] Wu, C., Y. Zhang, Y. Xu, B. Yan, and R. Xu, "Millimeter-wave waveguide-to-microstrip transition with a built-in DC/IF return path," *IEEE Transactions on Microwave Theory and Techniques*, Vol. 69, No. 2, 1295–1304, 2020.

[15] Zaman, A. U., V. Vassilev, H. Zirath, and N. Rorsman, "Novel low-loss millimeter-wave transition from waveguide-to-microstrip line suitable for MMIC integration and packaging," *IEEE Microwave and Wireless Components Letters*, Vol. 27, No. 12, 1098–1100, 2017.

[16] Wu, C., Y. Zhang, Y. Li, H. Zhu, F. Xiao, B. Yan, and R. Xu, "Millimeter-wave waveguide-to-microstrip inline transition using a wedge-waveguide iris," *IEEE Transactions on Microwave Theory and Techniques*, Vol. 70, No. 2, 1087–1096, 2021.

[17] Fang, R.-Y. and C.-L. Wang, "Miniaturized microstrip-to-waveguide transition using capacitance-compensated broadside-coupled microstrip line," *IEEE Transactions on Components, Packaging and Manufacturing Technology*, Vol. 3, No. 9, 1588–1596, 2013.

[18] Chuang, J.-K., R.-Y. Fang, and C.-L. Wang, "Compact and broadband microstrip-to-waveguide transition using antisymmetric tapered probes," *Electronics Letters*, Vol. 48, No. 6, 332–333, 2012.

[19] Varshney, A., V. Sharma, I. Elfergani, C. Zebiri, Z. Vujicic, and J. Rodriguez, "An inline V-band WR-15 transition using antipodal dipole antenna as RF energy launcher@ 60 GHz for satellite applications," *Electronics*, Vol. 11, No. 23, 3860, 2022.

[20] Varshney, A., V. Sharma, C. Nayak, A. K. Goyal, and Y. Massoud, "A low-loss impedance transformer-less fish-tail-shaped MS-to-WG transition for K-/Ka-/Q-/U-band applications," *Electronics*, Vol. 12, No. 3, 670, 2023.

[21] Varshney, A., V. Sharma, and A. Agarwal, "Next-generation MS-to-RWG interconnects for microwave and mm-wave communications using microstrip antenna as RF energy launcher @ 140 GHz," *Journal of The Institution of Engineers (India): Series B*, Vol. 104, No. 3, 749–756, 2023.

[22] Yoneda, N., R. Miyazaki, I. Matsumura, and M. Yamato, "A design of novel grooved circular waveguide polarizers," *IEEE Transactions on Microwave Theory and Techniques*, Vol. 48, No. 12, 2446–2452, Dec. 2000.

[23] Virone, G., R. Tascone, O. A. Peverini, and R. Orta, "Optimum-iris-set concept for waveguide polarizers," *IEEE Microwave and Wireless Components Letters*, Vol. 17, No. 3, 202–204, Mar. 2007.

[24] Bertin, G., B. Piovano, L. Accatino, and M. Mongiardo, "Full-wave design and optimization of circular waveguide polarizers with elliptical irises," *IEEE Transactions on Microwave Theory and Techniques*, Vol. 50, No. 4, 1077–1083, Apr. 2002.

[25] Albertsen, N. C. and P. Skov-Madsen, "A compact septum polarizer," *IEEE Transactions on Microwave Theory and Techniques*, Vol. 31, No. 8, 654–660, Aug. 1983.

[26] Behe, R. and P. Brachat, "Compact duplexer-polarizer with semicircular waveguide (antenna feed)," *IEEE Transactions on Antennas and Propagation*, Vol. 39, No. 8, 1222–1224, Aug. 1991.

[27] Ege, T. and P. McAndrew, "Analysis of stepped septum polarisers," *Electronics Letters*, Vol. 21, No. 24, 1166–1168, Nov. 1985.

[28] Wang, S.-W., C.-H. Chien, C.-L. Wang, and R.-B. Wu, "A circular polarizer designed with a dielectric septum loading," *IEEE Transactions on Microwave Theory and Techniques*, Vol. 52, No. 7, 1719–1723, Jul. 2004.

[29] Subbarao, B. and V. F. Fusco, "Compact coaxial-fed CP polarizer," *IEEE Antennas and Wireless Propagation Letters*, Vol. 3, 145–147, 2004.

[30] Jeon, K. J., K. J. Lee, T. K. Lee, J. W. Lee, and W. K. Lee, "Circular polarization generating coaxial to waveguide adapter for horn antenna," in *Proceedings of the Fourth European Conference on Antennas and Propagation*, 1–4, Barcelona, Spain, 2010.

[31] Stutzman, W. L. and G. A. Thiele, *Antenna Theory and Design*, John Wiley & Sons, 2012.

[32] Polat, H. K., M. D. Geyikoglu, and B. Cavusoglu, "Modeling and validation of a new reconfigurable patch antenna through equivalent lumped circuit-based design for minimum tuning effort," *Microwave and Optical Technology Letters*, Vol. 62, No. 6, 2335–2345, 2020.